J. Fluid Mech. (2003), *vol.* 496, *pp.* 129–138. © 2003 Cambridge University Press
DOI: 10.1017/S0022112003006438 Printed in the United Kingdom

The sensitivity of steady vortex breakdown bubbles in confined cylinder flows to rotating lid misalignment

By MARK C. THOMPSON AND KERRY HOURIGAN

Fluids Laboratory for Aeronautical and Industrial Research (FLAIR), Department of Mechanical Engineering, PO Box 31, Monash University, Melbourne, Victoria 3800, Australia

(Received 12 June 2003 and in revised form 28 August 2003)

Recent experimental observations using tracer visualization techniques have suggested that even for low Reynolds number flows, the steady vortex breakdown bubble in a torsionally driven cylinder is not axisymmetric and has an inflow/outflow asymmetry at its tail. These results seem to suggest that this type of vortex breakdown is closer in structure to that observed in the open vortex tube than previously thought. In this paper we examine numerically the effect of imperfections in the rig geometry, in particular quantifying the effect of a very slight misalignment between the axis of rotation of the end plate and the cylinder axis. It is shown that even slight misalignments, which are unlikely to be measurable experimentally, can produce the main details of non-axisymmetric open breakdown bubbles that have been observed in many experiments. This provides a resolution to the mismatch between the axisymmetric and closed bubble predictions of three-dimensional numerical simulations and stability analysis, and the observations of open bubbles often apparent even in carefully controlled experiments.

1. Introduction

The essential nature of vortex breakdown has been a matter of debate since the early days of its observation in flow over delta wings (Peckham & Atkinson 1957). The classic photograph by Lambourne & Bryer (1961) of vortex breakdown on a delta wing shows both a bubble-type and a spiral-type instability occurring on opposite sides of the wing simultaneously under apparently identical conditions. Since then, vortex breakdown has been studied in a variety of other situations: vortex tubes (Harvey 1962; Sarpkaya 1974, 1995; Faler & Leibovich 1977, 1978; Escudier & Zehnder 1982; Brucker & Althaus 1995), confined cylinders with rotating disk lids (Vogel 1968; Escudier 1984; Hourigan, Graham & Thompson 1995; Spohn, Mory & Hopfinger 1998), tornado generators (Khoo *et al.* 1997), free swirling air jets (Farokhi, Taghavi & Rice 1988; Panda & McLaughlin 1994), and the swirling water jet (Billant, Chomaz & Huerre 1998). The differing environments in which vortex breakdown occurs, and the variety of breakdown characteristics observed, have led to dispute over the fundamental nature of the breakdown process.

Many researchers who have studied vortex breakdown in pipes or from delta wings, have either explicitly or implicitly assumed that vortex breakdown has two essential features, namely asymmetry and an open structure; however, neither of these characteristics had been apparent in the recirculation zones found in the lower Reynolds number range for the confined cylinder flow case. As Leibovich (1978,

https://doi.org/10.1017/S0022112003006438 Published online by Cambridge University Press

1984, 1999) has frequently emphasized, the assumption of axisymmetry has been used extensively in theoretical and numerical studies even though it is not observed for the flow that motivated many of these studies, namely flow over a delta wing, nor is it observed in the idealized case of the vortex tube. In the latter case, closed bubbles (Types 0 and 1 in the classification of Faler & Leibovich 1977) are observed which, although generally of an axisymmetric nature, possess an asymmetric spiralling tail with inflow/outflow. Furthermore, Goldshtik & Hussain (1998) argue that the confined cylinder flow should not be termed vortex breakdown, but probably internal separation, as jumps and hysteretic transitions are not observed. At least in the lower Reynolds number range, the confined cylinder flow has appeared to be robustly axisymmetric with closed steady bubbles, with near-axis separation zones appearing gradually, and not discontinously, as the control parameters are changed.

A study by Spohn *et al.* (1998) has offered a markedly different view, asserting that there is a far closer similarity between the flows in the confined cylinder and the vortex tube than previously thought. Their experiments used three different flow visualization techniques. First, an electrolytic precipitation method, used previously by Honji, Taneda & Tatsuno (1980), was adapted to the confined flow. Second, complementary visualization was undertaken using the fluorescent dye technique employed previously by, for example, Escudier (1984) and Hourigan *et al.* (1995). Third, some limited particle image velocimetry was undertaken. The essence of the results of Spohn *et al.* (1998) are that vortex breakdown bubbles in the confined case are not closed but are *steady open* bubbles with permanent inflow and outflow at the tail. Furthermore, it is shown that the flows are not perfectly symmetric. It is claimed that the observed asymmetry is real and is not caused by inadequacies of the visualization techniques; the imperfections in their installation were so small that even reassembling of the rig led to no differences in the flow structures observed. They conclude that it is not justified to assume that unsteadiness is a basic ingredient of vortex breakdown, and that the flow in the confined cylinder leads to breakdown bubbles similar to those observed in open tubes.

Considering the large number of studies, conducted on vortex breakdown in confined cylinders, the observations and conclusions of Spohn *et al.* (1998) are potentially profound and far-reaching. Their observations conflict with previous understanding of the simplest form of vortex breakdown, the low Reynolds number steady axisymmetric flow in a confined cylinder. For example, in closed cylinders with an aspect ratio of 2.0, Sorensen & Christensen (1995) observe that the flow remains axisymmetric even above the first Hopf bifurcation up to $Re = 3000$. In particular, Spohn *et al.* (1998) concluded that the downstream region of the breakdown bubbles displayed distinct asymmetry whereas the upstream region, like the vortex tube case, was axisymmetric. They point out that asymmetric structures on the downstream side of breakdown bubbles are also visible on photographs presented by Escudier (1984), Boehme, Rubart & Stenger (1992) and Husain, Hussain & Goldshtik (1995).

Some recent numerical studies support the experimental predictions of open bubbles. Sotiropoulos & Ventikos (1998, 2001), and Sotiropoulos, Ventikos & Lackey (2001) reported on numerical simulations of vortex breakdown in a torsionally driven cylinder which predicted a steady open bubble similar to that observed in the visualizations of Spohn *et al.* (1998) using precipitate. They used a finite-difference method based on generalized non-orthogonal Cartesian coordinates which was second-order in space and time. Interestingly, their mesh possessed fourfold rotational azimuthal symmetry. This symmetry is also apparent in the calculated flow fields at higher Reynolds numbers (e.g. $Re = 6000$). However, at $Re = 1850$ it appears

https://doi.org/10.1017/S0022112003006438 Published online by Cambridge University Press

that the breakdown bubble possesses single *spiral-in* and *spiral-out* saddle points. More recently Sotiropoulos, Webster & Lackey (2002) have produced experimental visualizations supporting the open-bubble visualizations of Spohn *et al.* (1998) as part of a study on chaotic particle advection. They show the effect on the downstream bubble structure of a spinning lid misalignment of 0.4°. Furthermore, they find that even with the lid aligned correctly, the steady bubble still has an open structure.

The possible causes for the observed open and asymmetrical nature of the bubbles in the closed cylinder include the following: asymmetries in rig itself, such as deviations from axisymmetric geometry or non-uniformity of disk rotation; the detection of flow instabilities that have not been observed previously or captured by simulations; inaccurate depiction of the flow field by the visualization technique employed. *A priori*, it is not obvious that lack of axisymmetry severe enough to induce measurable flow asymmetry is present across the large number of rigs used for confined cylinder flows. This assumption is specifically examined in this paper. As for the appearance of non-rotating modes, a stationary mode would be expected to exist at only one spin rate and not over a range as observed by Spohn *et al.* (1998). A preliminary investigation on the influence of the visualization techniques is given in Hourigan & Thompson (2001), and an expansion of that work will form the basis of a future article.

In this article, a plausible resolution of the conundrum between the typical axisymmetric bubble predictions of fully three-dimensional high-resolution simulations, and experimental and some numerical *open-bubble* visualizations by different investigators is suggested. First, a restricted stability study is undertaken to reinforce the results of Gelfgat, Bar-Yoseph & Solan (2001) verifying that the bubble is only unstable to non-axisymmetric modes at Reynolds numbers higher than those that apparently give open bubbles in some experiments. Second, a study is undertaken into the effect of misalignment of the rotating lid axis with the cylinder axis, which represents one of the possible imperfections in the construction of experimental rigs. Perhaps surprisingly, it is demonstrated that vortex breakdown in a confined cylinder is so sensitive to this slight misalignment that experimental generation of vortex breakdown in this apparatus will almost invariably result in an open bubble.

2. Numerical method

The outcomes of two numerical studies are reported in this article. These simulations employed a spectral-element method for axisymmetric geometries. A spectral-element discretization was used in the (r, z)-planes and, for the three-dimensional simulations, a Fourier expansion in the θ-direction. The three-dimensional form of the code has been described and validated extensively previously for both Cartesian and axisymmetric problems requiring high resolution (Thompson, Hourigan & Sheridan 1996; Thompson, Leweke & Provansal 2001; Sheard, Thompson & Hourigan 2003).

2.1. *Resolution study*

Since an aim of this study is to demonstrate that, for a 'perfect geometry', the transition to three-dimensional flow occurs at much higher Reynolds numbers than indicated by the experimental study of Spohn *et al.* (1998), and the numerical studies of Sotiropoulos & Ventikos (1998, 2001), and Sotiropoulos *et al.* (2001), it is important to demonstrate the solutions presented here are adequately resolved. The spectral-element mesh used for all the time-dependent simulations is shown in figure 1. The spinning lid is positioned at the left-hand boundary of the domain. Compression of

https://doi.org/10.1017/S0022112003006438 Published online by Cambridge University Press

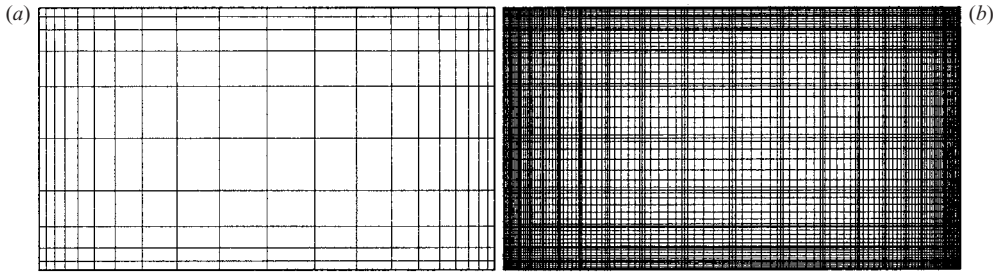


FIGURE 1. (*a*) Two-dimensional spectral-element mesh used for the simulations. Elements are further subdivided into $N_x \times N_y$ node points. (*b*) The internal nodes within the elements for $N_x \times N_y = 5 \times 5$; this was used for the majority of the simulations. For the three-dimensional simulations, the mesh is extended in the azimuthal direction using a Fourier expansion. The bottom line marks the cylinder centreline.

$N_x \times N_y$	Δt	S_{min} (breakdown bubble)	S_{max} (primary recirculation)	% error (S_{max})
3×3	0.01	-0.589×10^{-4}	0.7689×10^{-2}	1.56
4×4	0.01	-0.501×10^{-4}	0.7806×10^{-2}	0.06
4×4	0.005		0.7808×10^{-2}	
4×4	0.0025		0.7809×10^{-2}	
5×5	0.01	-0.489×10^{-4}	0.7809×10^{-2}	0.03
7×7	0.01	-0.486×10^{-4}	0.7811×10^{-2}	0.00
9×9	0.01	-0.485×10^{-4}	0.7811×10^{-2}	—

TABLE 1. Convergence of the axisymmetric solution against spectral-element order and timestep. The $N_x \times N_y = 9 \times 9$ solution is assumed to be spatially converged for the purposes of estimating the solution error.

the mesh towards the boundaries has been implemented, to assist with resolving the Ekman layer at the spinning lid and Stewartson layer on the cylinder wall. Internally, each element is subdivided into $N_x \times N_y$ nodes. For the current resolution study this number was varied between $N_x \times N_y = 3 \times 3$ and 9×9.

With the Reynolds number set to 1850, axisymmetric solutions were evolved until the maximum change in any velocity component anywhere in the domain was below 1.0×10^{-9}. This was sufficient to achieve four-significant-figure accuracy for the streamfunction, verified using a stronger convergence criterion. Table 1 shows the minimum (S_{min}) and maximum (S_{max}) streamfunction over the domain as a function of mesh resolution. These numbers correspond to the strengths of the main recirculation within the cylinder and the vortex breakdown bubble. The rapid convergence of the method is clearly demonstrated. Assuming the $N_x \times N_y = 9 \times 9$ solution is converged to better than four-digit accuracy, the solution error in the predicted maximum streamfunction is less than 0.1% for a mesh using only 4×4 elements. Further tests were conducted to ensure that the very thin Ekman layer at the spinning lid was also well resolved with the 4×4 mesh. Note that the predicted values of S_{min} and S_{max} are consistent with the independent highly resolved finite-element simulations for this same case. The second-order time-splitting method used for the time integration induces a time-stepping error even for the steady-state solution. Table 1 also shows a convergence study for dependence on timestep: the difference between the $\Delta t = 0.01$

https://doi.org/10.1017/S0022112003006438 Published online by Cambridge University Press

Mode	Re_{crit}	Re^{*}_{crit}
unsteady axisymmetric	2650 ± 10	2650
$m = 2$ non-axisymmetric	2815 ± 10	2850
$m = 1$ non-axisymmetric	3260 ± 20	3250
$m = 3$ non-axisymmetric	3440 ± 20	3500

TABLE 2. Critical Reynolds numbers for aspect ratio 1.75 cylinder. Stability was tested for $m \leqslant 8$, $Re \leqslant 3500$; hence, higher-order modes are only unstable above this value. Re^{*}_{crit} represent values from Gelfgat *et al.* (2001) extracted from their figure 1. Graphical accuracy only allows these values to be estimated to within approximately ± 50.

and 0.0025 solutions is less than 0.04%. Note that $\Delta t = 0.01$ corresponds to 628 timesteps per lid rotation.

In conclusion, this resolution study indicates that using a mesh with 5×5 elements and a timestep of 0.01 should lead to a global error of 0.1% or less. This combination of temporal and spatial resolution was used for the three-dimensional simulations and stability analysis described in the following sections. Importantly, because a Fourier expansion is used in the azimuthal direction, this results in arbitrary rotational symmetry and hence is unlikely to lead to artificial generation of non-axisymmetric flows, which may be possible with meshes without this symmetry.

2.2. *Stability analysis*

Numerical simulations typically predict that the flow in a spinning lid rig leads to steady axisymmetric vortex breakdown prior to becoming unsteady or becoming unstable to non-axisymmetric modes. These direct simulations are supported by linear stability analysis (Gelfgat *et al.* 1996, 2001) which predicts the same behaviour. Here, the stability of axisymmetric base flows is determined again using a numerical stability code derived from the three-dimensional spectral/spectral-element code described previously. The stability is determined by solving the linearized problem. The velocity and pressure fields are expanded about the axisymmetric base flow for a particular Reynolds number. The growth rate of non-axisymmetric modes is directly determined by time integration of the linearized problem with regular renormalization of the perturbation modes. The approach allows the stability of both stationary and rotating modes to be determined. In addition, the stability of the steady base flow to time-dependent behaviour is simultaneously determined through the time-integration of the perturbed base flow. As noted above, the aim is to verify that the steady axisymmetric base flow is stable prior to the development of non-axisymmetric flow at higher Reynolds numbers, or equivalently, that the axisymmetric breakdown flow occurs prior to non-axisymmetric flow.

At $Re = 1850$, both the unsteady axisymmetric mode and the azimuthal varying modes have negative growth rates. The critical Reynolds numbers for the different modes are given in table 2. These values are in good agreement with those given in Gelfgat *et al.* ((2001, figure 1), with values duplicated in table 2). In addition, the non-axisymmetric modes do not have non-zero azimuthal wave speed, i.e. they are not stationary. In particular, the $m = 1$ mode is a *rotating* mode that first becomes unstable at a Reynolds number of 3260. Also of interest (but not shown in the table), the $m = 4$ mode, evident in the simulations of Sotiropoulos & Ventikos (1998), does not become linearly unstable on the axisymmetric base flow until the Reynolds number exceeds 5000.

https://doi.org/10.1017/S0022112003006438 Published online by Cambridge University Press

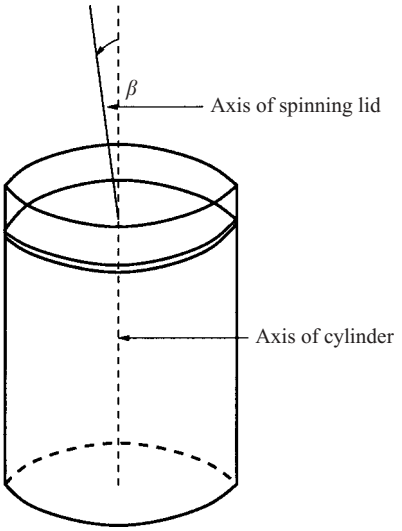


FIGURE 2. Diagram showing misalignment of the rotating endwall with the cylinder axis.

2.3. *Three-dimensional simulations*

A three-dimensional simulation of the flow at $\mathrm{Re} = 1850$ was undertaken to independently verify that the final asymptotic three-dimensional time-dependent state is indeed axisymmetric. The mesh used was the same as for the two-dimensional resolution study extended to three dimensions using a Fourier expansion in the azimuthal direction. Typically, 32 Fourier planes were used. The flow was evolved from an initially stationary state. In order to accelerate the development of any three-dimensionality, a white noise perturbation of relative amplitude 10^{-3} was added to each velocity component at each node after the first few timesteps. The flow field was subsequently evolved for a time corresponding to approximately 100 lid revolutions. All Fourier components (except the zeroth mode) decayed quickly (verified by monitoring the decay rates) leaving the flow in a purely axisymmetric state.

2.4. *Effect of misalignment of the rotating endwall*

In this section, the effect of one rig non-axisymmetry on the development of an otherwise axisymmetric bubble is considered. Naturally, there are many possible rig imperfections that may affect the development of the breakdown bubble; however, to limit parameters investigated, this study is restricted to the alignment of the spinning endwall. In particular, the effect of a slight angular misalignment (β) of the axis of rotation with the cylinder axis is considered as shown in figure 2. One effect of the misalignment of axes is that there is a small azimuthally varying induced axial velocity at the spinning endwall. As previously described, the current three-dimensional code requires an axisymmetric geometry, although it can treat fully three-dimensional flows. So to investigate the effect of misalignment, the induced axial velocity at the spinning endwall is imposed, while still maintaining the strict axisymmetric geometry. While an approximation, it should accurately reveal the effect of this misalignment.

The results are surprising. The flow evolves to a steady state with an open bubble. After it has reached its equilibrium state, tracers are introduced $0.01D$ from the stationary endwall (where D is cylinder diameter). The initial positions are equi-distributed in angle at a radius of $0.01D$ from the cylinder axis. The misalignment

https://doi.org/10.1017/S0022112003006438 Published online by Cambridge University Press

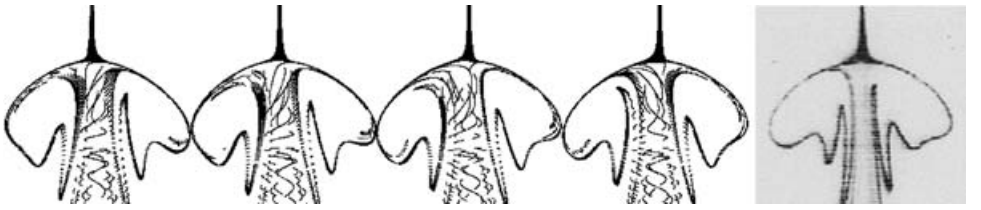


FIGURE 3. Cross-sections through the breakdown bubble at $Re = 1850$. The first four images are predicted visualizations at azimuthal angles of 0, 45°, 90° and 135°, respectively. The misalignment angle is 0.1°. The fifth is an electrolytic precipitation visualization from Spohn *et al.* (1998), showing excellent agreement with the predictions. The structure in the cores shown in the numerical visualizations is an artifact of limiting the number of particles injected to make the computations manageable.

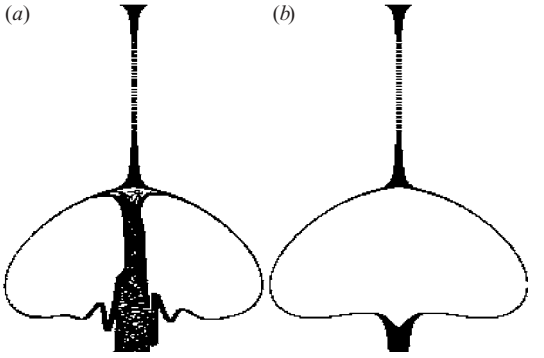


FIGURE 4. (*a*) Effect of reducing the misalignment to 0.01°.
(*b*) Visualization with no misalignment.

angle for this simulation is $\beta = 0.1°$. For the apparatus used by Spohn *et al.* (1998), this corresponds to a mismatch in the axial position at the cylinder wall relative to the axis of the rotating endwall of less than 0.1 mm. Figure 3 shows various slices through the bubble, after the particles have convected past (and also into) the bubble. These snapshots bear a remarkable resemblance to the visualizations of Spohn *et al.* (1998) using electrolytic precipitation. A figure from that paper is reproduced in figure 3 for comparison. Clearly, folding of the base of the bubble is less in the experimental visualization, indicating that the misalignment angle may be less than 0.1°.

Figure 4 shows the simulated tracer pattern for $\beta = 0.01°$. Even in this case there is still some folding at the downstream end of the bubble. For comparison, tracers for the perfectly aligned case are also shown which show that axisymmetry is maintained.

As a final comparison, Spohn *et al.* (1998) show a time history of the precipitated particles as they first pass around the breakdown bubble. Figure 5 shows a comparison of these experimental visualizations and the numerical visualization predictions at approximately the same times. For the simulations, the misalignment angle was chosen to be 0.03°, since the previous results displayed in the figures suggest that the best fit to the experimental visualizations would be for β in the range $(0.01°, 0.1°)$. Whilst displaying the important features, the comparison is not perfect. In the experiments, the precipitate was released from the sidewalls of the cylinder by an embedded wire. In the simulations, the release was centred on the cylinder axis close to the top wall to limit the computer time since convection of particles in the wall boundary layers is very slow. There may be other imperfections in the experiments, such as the alignment

https://doi.org/10.1017/S0022112003006438 Published online by Cambridge University Press

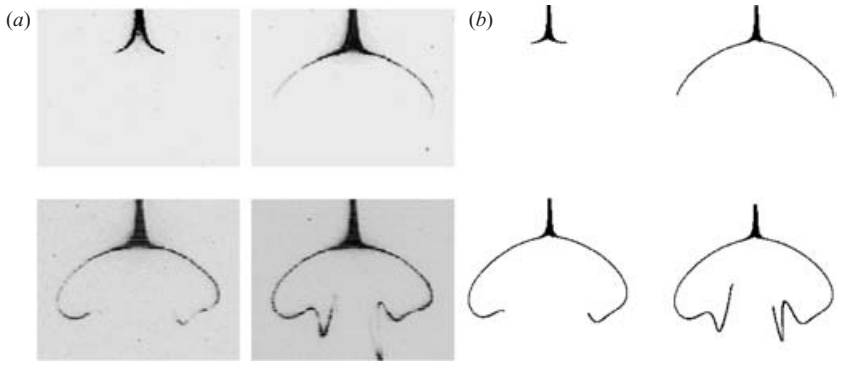


FIGURE 5. (*a*) Views of the structure of the vortex breakdown bubble as outlined by convecting precipitate at four consecutive times. (Reproduced from figure 9 of Spohn *et al.* 1998). (*b*) Comparison views from the numerical simulations at approximately the corresponding times. $Re = 1850$, $\beta = 0.03°$.

of other surfaces, non-planar endwalls, non-circularity of the cylinder, uncertainties in the exact viscosity, etc, which make an exact reconstruction impossible (given the sensitivity of this flow). Nevertheless, this sequence clearly shows a remarkably similar folding at the rear of the bubble to that observed in experiments.

3. Conclusions

Many experimental visualizations of vortex breakdown have been performed by very careful experimentalists. For example, Spohn *et al.* (1998) specifically state their apparatus was disassembled and reassembled giving the same open bubble structure as before. As stated above, this loss of rotational symmetry at the rear of breakdown bubbles in the spinning lid rig is common in many articles showing experimental visualizations of vortex breakdown. Hourigan & Thompson (2001), and Hourigan *et al.* (1995) showed it could be attributed to off-axis injection of tracer particles perhaps coupled with non-zero dye diffusivity which allows dye to cross separating streamlines and hence enter the bubble. In this case, however, while this effect may be a contributing factor, it seems likely that the dominant cause is slight errors in the construction of the rig. To limit the parameters to be investigated, this study is restricted to errors in the alignment of the spinning lid axis with the cylinder axis.

The effect on the breakdown bubble of even a very minor misalignment is shown to be substantial and can lead to characteristic folds on the downstream side of the bubble very similar to those observed in the experiments. A reasonable conclusion is that this is a possible mechanism leading to the distinctive folds observed in the experimental electrolytic precipitation visualizations of Spohn *et al.* (1998). The stability analysis supports this conjecture. For a perfect geometry, it clearly shows that vortex breakdown first occurs as an axisymmetric bubble prior to becoming unstable to non-axisymmetric modes at higher Reynolds numbers. Even after the flow becomes non-axisymmetric, it does so to rotating modes and not stationary (azimuthal) modes as observed by Spohn *et al.* (1998).

Perhaps the biggest surprise is the magnitude of the misalignment required to generate a clearly open bubble. The simulations indicate that results similar to the experimental results of Spohn *et al.* (1998) are obtained for a misalignment angle of approximately 0.03°; with a misalignment of just 0.01°, the downstream folds are still

https://doi.org/10.1017/S0022112003006438 Published online by Cambridge University Press

clearly visible. Even with careful alignment of the components of an experimental rig during construction it would seem that this tolerance criterion is unlikely to be met. The vortex breakdown flow is clearly very sensitive. In retrospect, this may not be surprising, since the streamlines must diverge rapidly away from the axis as the fluid approaches the bubble and then again converge rapidly towards the axis after the fluid passes the bubble.

The results presented in this paper highlight the methodology and care required in both experiments and simulations, especially in the interpretation of results. From one point of view the results indicate that numerical simulations of idealized flows are not necessarily a good representation of even high-quality experiments purporting to model the same idealized flow. Recently, Lucor *et al.* (2003) have applied stochastic modelling methods based on polynomial chaos to try include some of these effects in the modelling process. Alternatively, the results may be taken as a warning to experimentalists that they may not be producing results entirely relevant to the problem they think they are modelling. Finally, it is noted that we have found recirculation regions in other contexts to be extremely sensitive to flow perturbations. For example, the vortex shedding from the separation bubble at the semi-circular leading edge of a plate can be locked to acoustic particle velocity perturbations as low as 0.0001 of the free-stream velocity (Welsh *et al.* 1990).

The authors gratefully acknowledge the funding from an Australian Research Council Large Grant for this research. In addition, we would like to acknowledge the support of the Victorian and Australian Partnerships for Advanced Computing (VPAC & APAC), which allowed many of the numerical studies to be performed.

REFERENCES

Billant, P., Chomaz, J.-M. & Huerre, P. 1998 Experimental study of vortex breakdown in swirling jets. *J. Fluid Mech.* **376**, 183–219.

Boehme, G., Rubart, L. & Stenger, M. 1992 Vortex breakdown in shear-thinning liquid: experiment and numerical simulation. *J. Non-Newtonian Fluid Mech.* **45**, 1–19.

Brücker, C. & Althaus, W. 1995 Study of vortex breakdown by particle tracking velocimetry (PTV), Part 3: Time-dependent structure and development of breakdown modes. *Exps. Fluids* **18**, 174–186.

Escudier, M. P. 1984 Observations of the flow produced in a cylindrical container by a rotating endwall. *Exps. Fluids* **2**, 189–196.

Escudier, M. P. & Zehnder, N. 1982 Vortex-flow regimes. *J. Fluid Mech.* **115**, 105–121.

Faler, J. H. & Leibovich, S. 1977 Disrupted states of vortex flow and vortex breakdown. *Phys. Fluids* **20**, 1385–1400.

Faler, J. H. & Leibovich, S. 1978 An experimental map of the internal structure of a vortex breakdown. *J. Fluid Mech.* **86**, 313–335.

Farokhi, S., Taghavi, R. & Rice, E. J. 1988 Effect of initial swirl distribution on the evolution of a turbulent jet. *AIAA J.* **27**, 700–706.

Gelfgat, A. Yu., Bar-Yoseph, P. Z. & Solan, A. 1996 Stability of confined swirling flow with and without vortex breakdown. *J. Fluid Mech.* **311**, 1–36.

Gelfgat, A. Yu., Bar-Yoseph, P. Z. & Solan, A. 2001 Three-dimensional instability of axisymmetric flow in a rotating lid-cylinder enclosure. *J. Fluid Mech.* **438**, 363–377.

Goldshtik, M. & Hussain, F. 1998 Analysis of inviscid vortex breakdown in a semi-infinite pipe. *Fluid Dyn. Res.* **23**, 189–234.

Harvey, J. K. 1962 Some observations of the vortex breakdown phenomenon. *J. Fluid Mech.* **13**, 585–592.

https://doi.org/10.1017/S0022112003006438 Published online by Cambridge University Press

Honji, H., Taneda, S. & Tatsuno, M. 1980 Some practical details of the electrolytic precipitation method of flow visualisation. *Rep. Res. Inst. of Appl. Mech.*, XXVIII. Kyushu University, Fukuoka, Japan.

Hourigan, K., Graham, L. W. & Thompson, M. C. 1995 Spiral streaklines in pre-vortex breakdown regions of axisymmetric swirling flows. *Phys. Fluids* **7**, 3126–3128.

Hourigan, K. & Thompson, M. C. 2001 Structure of vortex beakdown in a torsionally driven cylinder at low Reynolds number. *Proc. 14th Australasian Fluid Mechanics Conference, Adelaide University, 9–14 December* (ed. B. Dally), pp. 601–604.

Husain, H. S., Hussain, F. & Goldshtik, M. 1995 Anomalous separation of homogeneous particle-fluid mixtures: further observations. *Phys. Rev.* E **52**, 4909–4923.

Khoo, B. C., Yeo, K. S., Lim, D. F. & He, X. 1997 Vortex breakdown in an unconfined vortical flow. *Expl Therm. Fluid Sci.* **14**, 131–148.

Lambourne, N. C. & Bryer, D. W. 1961 The bursting of leading-edge vortices: some observations and discussion of the phenomenon. *Aero. Res. Counc. R & M* 3282 1–36.

Leibovich, S. 1978 The structure of vortex breakdown. *Annu. Rev. Fluid Mech.* **10**, 221–246.

Leibovich, S. 1984 Vortex stability and breakdown: survey and extension. *AIAA J.* **22**, 1192–1206.

Leibovich, S. 1999 Sensitivity of vortex flows and vortex breakdown to farfield conditions. *AIAA Paper* 99–3765.

Lucor, Xiu, D. Su, C. H. & Karniadakis, G. E. 2003 Predictability and uncertainty in CFD. *Intl J. Num. Meth. Fluids* (in press).

Panda, J. & McLaughlin, D. K. 1994 Experiments on the instabilities of a swirling jet. *Phys. Fluids* **6**, 263–276.

Peckham, D. H. & Atkinson, S. A. 1957 Preliminary results of low speed wind tunnel tests on a gothic wing of aspect ratio 1.0. *ARC Tech. Rep. CP Aero.* 2504.

Sarpkaya, T. 1974 Effect of the adverse pressure gradient on vortex breakdown. *AIAA J.* **12**, 602–607.

Sarpkaya, T. 1995 Turbulent vortex breakdown. *Phys. Fluids* **7**, 2301–2303.

Sheard, G. J., Thompson, M. C. & Hourigan, K. 2003 From spheres to circular cylinders: the stability and flow structures of bluff ring wakes. *J. Fluid Mech.* **492**, 147–180.

Sorensen, J. N. & Christensen, E. A. 1995 Direct numerical simulation of rotating fluid flow in a closed cylinder. *Phys. Fluids* **7**, 764–778.

Sotiropoulos, F. & Ventikos, Y. 1998 Transition from bubble-type vortex breakdown to columnar vortex in a confined swirling flow. *Intl J. Heat Fluid Flow* **19**, 446-458.

Sotiropoulos, F. & Ventikos, Y. 2001 The three-dimensional structure of confined swirling flows with vortex breakdown. *J. Fluid Mech.* **426**, 155–175.

Sotiropoulos, F., Ventikos, Y. & Lackey, T. C. 2001 Chaotic advection in a three-dimensional stationary vortex-breakdown bubble: Sil'nikov's chaos and the devil's staircase. *J. Fluid Mech.* **444**, 257–297.

Sotiropoulos, F., Webster, D. R. & Lackey, T. C. 2002 Experiments on Lagrangian transport in steady vortex-breakdown bubbles in a confined swirling flow. *J. Fluid Mech.* **466**, 215–248.

Spohn, A., Mory, M. & Hopfinger, E. J. 1998 Experiments on vortex breakdown in a confined flow generated by a rotating disc. *J. Fluid Mech.* **370**, 73–99.

Thompson, M. C., Hourigan, K. & Sheridan, J. 1996 Three-dimensional instabilities in the wake of a circular cylinder. *Expl Therm. Fluid Sci.* **12**, 190–196.

Thompson, M. C., Leweke, Th. & Provansal, M. 2001 Kinematics and dynamics of sphere wake transition. *J. Fluids Struct.* **15**, 575–585.

Vogel, H. U. 1968 Experimentelle Ergebnisse ber die laminare Strömung in einen zylindrischen Gehäuse mit darin rotierender Scheibe. *Tech. Rep. Bericht* 6. Max-Plank-Inst.

Welsh, M. C., Hourigan, K., Welch, L. W., Downie, R. J., Thompson, M. C. & Stokes, A. N. 1990 Acoustics and experimental methods: the influence of sound and heat transfer. *Expl Therm. Fluid Sci.* **3**, 138–152.

https://doi.org/10.1017/S0022112003006438 Published online by Cambridge University Press